Faraday rotation and ellipticity spectroscopy between excited states of Rb vapor: Theory and experiment

Chenxu Liu⬤, Yalong Hai⬤, and Anhong Dang*

School of Electronics, Peking University, Beijing 100871, China

The Faraday rotation and ellipticity spectra of rubidium $5P_{3/2} \to 4D_{5/2}$ transition in a magnetic field have been calculated and experimentally measured. By using the rotating quarter-wave plate method, the Stokes parameters of the $5P_{3/2} \to 4D_{5/2}$ near-resonant probe light are measured to obtain the Faraday rotation and the ellipticity. The variation of the rotation and the ellipticity spectra is analyzed in different magnetic fields, temperatures, and pump powers. The polarization rotation over 50 deg in 1529 nm with negligible elliptical distortion is obtained. Our study of the Faraday effect between excited states of atoms broadens the available wavelength of the Faraday effect in applications.

I. INTRODUCTION

The study of optical nonreciprocity attracts increasing interest with the development of laser technology [1]. Optical nonreciprocity devices such as isolators [2,3] and circulators [4] play an important role in optical signal processing [5–7] and quantum networks [8,9]. The magneto-optical Faraday effect can change the polarization state of the optical signal by breaking the absorption and dispersion symmetry of the σ^+ and σ^- circular polarization components of the transitions of atoms [10–12], which is a common way to obtain polarization rotational optical nonreciprocity. The manipulation of optical signals can be accomplished at the optical layer without the conversion of light-electricity-light [13,14]. By introducing an additional optical field, the polarization state of the optical signal can be controlled [15] for applications as all-optical switching [16,17], dynamic wave plates [18], and tunable beam splitters [19] in fiber optic [20] and all-optical networks [21].

The applications of the magneto-optical Faraday effect in vapor cells are limited by the transition wavelength of atoms. Currently, most of the works manipulate the polarization state for the optical signal at the wavelength of the direct transitions of atoms [2,13,15,18,19,22,23], while few works investigate the wavelength of the optical signal corresponding to the transitions between excited states of atoms. In comparison with the direct transitions, the transitions between excited states have flexible wavelength selection ranges, which can provide more adaptable scenarios for optical devices. In this study, we investigated the Faraday effects of the rubidium $5P_{3/2} \to 4D_{5/2}$ transition with the wavelength of 1529 nm. This wavelength is in the vicinity of the C band for wavelength-division multiplexing [24] of optical fiber communications for a low transmission loss in optical fiber and corresponds to the atmospheric window in free-space optical communications [25]. It can also apply to quantum networks in the 1.5-μm waveband [26,27], which is a widely used wavelength band in modern optical communications.

In the Faraday effect of direct transitions of atoms, it has achieved a 90° polarization rotation of off-resonant optical signals with negligible distortion [13]. However, it is difficult to obtain a high concentration of the intermediate excited state atoms because pumping is needed in transitions between excited states [28], so it is hard to obtain a large off-resonant rotation. In this study, the polarization rotation control of rubidium $5P_{3/2} \to 4D_{5/2}$ near-resonant light of the wavelength 1529 nm with negligible elliptical distortion is obtained. Our work bridges the void in the study of the Faraday effect between excited states and expands its wavelength range for applications on optical nonreciprocity.

The structure of this paper is as follows. In Sec. II, the theoretical two-photon absorption process of Faraday rotation and ellipticity in magnetic field is demonstrated. In Sec. III, we describe the experimental apparatus, giving theory and experimental results for different cases in Sec. IV. The control of polarization rotation under the variation of pump power is obtained in Sec. IV.

II. THEORY

As shown in Fig. 1, the $5S_{1/2}$, $5P_{3/2}$, and $4D_{5/2}$ states are the ground state (g), the intermediate excited state (e), and the doubly excited state (d), respectively. The decay rates of the $5P_{3/2}$ state and the $4D_{5/2}$ state are Γ_1=6.05MHz [29] and Γ_2= 1.97MHz [30], respectively.

The eigenvalues and eigenstates of those three states can be calculated by the coupled basis $|I, J, F, m_F\rangle$, so the transition probability σ_{ge} and σ_{ed} of the eigenvalues between the upper and lower energy levels is obtained. The calculation details are shown in the Appendix.

The concentration of the sublevels in intermediate excited state is proportional to the transition probability when the pump light is relatively low. Considering the Doppler effect
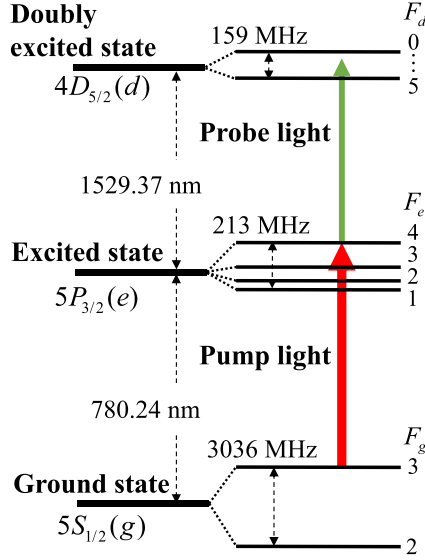
*ahdang@pku.edu.cn

FIG. 1. The schematic diagram of the $5S_{1/2} \rightarrow 5P_{3/2} \rightarrow 4D_{5/2}$ hyperfine structure of ^{85}Rb.

of pumping, the atom concentration N_{ge} pumped from the eigenstates of the transition $g \rightarrow e$ is

$$N_{ge} = \exp\left(-\frac{4\ln 2(\omega_{\text{pump}} - \omega_{ge})^2}{\Delta\omega_D^2}\right) \times \frac{\sigma_{ge}^2 N_e}{\sum_g \sum_e \sigma_{ge}^2}, \quad (1)$$

where ω_{pump} is the angular frequency of pump light, ω_{ge} is the angular frequency of the transition branch between the sublevels of the $g \rightarrow e$ states, $\Delta\omega_D$ is the Doppler width, and N_e is the total concentration of the intermediate excited state atoms.

The susceptibility of the transition branch among the sublevels of the $g \rightarrow e \rightarrow d$ states can be expressed as [29]

$$\chi_{g \rightarrow e \rightarrow d} = \frac{\sigma_{ed}^2 N_{ge}}{\hbar\epsilon_0} \times \frac{1}{(\omega_{\text{probe}} - \omega_0) + i\Gamma_L/2}. \quad (2)$$

The real and the imaginary parts of the susceptibility characterize the dispersion and the absorption profile, respectively. Here Γ_L is the Lorentzian linewidth of the "e" state including collisional broadening, ω_{probe} is the angular frequency of the probe light, and ω_0 is the equivalent central angular frequency under the wavelength mismatch effect:

$$\omega_0 = \omega_{ed} \pm \frac{\omega_{\text{probe}}}{\omega_{\text{pump}}}(\omega_{\text{pump}} - \omega_{ge}), \quad (3)$$

where the symbols $+$ and $-$ represent the copropagating and the counterpropagating of the pump light and the probe light, respectively. ω_{ed} is the angular frequency of the transition branch between the sublevels of the $e \rightarrow d$ states.

The total susceptibility in the vapor cell is the sum of the susceptibility of the corresponding eigenstates of the three states:

$$\chi = \sum_g \sum_e \sum_d \chi_{g \rightarrow e \rightarrow d}. \quad (4)$$

For the vapor cell under the longitudinal magnetic field, the $\sigma^\pm$ circular lights have different susceptibility $\chi_\pm$, so they

have different absorption $\alpha_\pm$ (circular dichroism) and different refractive index $n_\pm$ (circular birefringence) [31]:

$$\alpha_\pm = \frac{\omega_{\text{probe}}}{c}\text{Im}(\chi_\pm), \quad (5)$$

$$n_\pm = 1 + \frac{1}{2}\text{Re}(\chi_\pm). \quad (6)$$

The complex amplitudes $E_\pm$ of the $\sigma^\pm$ circular polarization components of the exiting probe light are

$$\begin{pmatrix} E_+ \\ E_- \end{pmatrix} = \begin{pmatrix} E_{0+}\cos(\omega_{\text{probe}}t + \varphi_+) \\ E_{0-}\cos(\omega_{\text{probe}}t + \varphi_-) \end{pmatrix}$$
$$= \frac{\sqrt{2I_0}}{2}\begin{pmatrix} \exp\left(-\frac{1}{2}\alpha_+ L\right)\cos\left(\omega_{\text{probe}}t + \frac{\omega}{c}n_+ L\right) \\ \exp\left(-\frac{1}{2}\alpha_- L\right)\cos\left(\omega_{\text{probe}}t + \frac{\omega}{c}n_- L\right) \end{pmatrix}, \quad (7)$$

where I_0 is the light intensity and L is the cell length.

The Stokes parameters of the elliptically polarized light exiting the cell can be expressed in terms of the rotation angle (orientation angle) θ, the elliptical angle δ, and the total light intensity I_0, and also in terms of the complex amplitudes of the $\sigma^\pm$ circular polarization components [32]:

$$\begin{pmatrix} S_0 \\ S_1 \\ S_2 \\ S_3 \end{pmatrix} = \begin{pmatrix} I_0 \\ I_0\cos 2\delta\cos 2\theta \\ I_0\cos 2\delta\sin 2\theta \\ I_0\sin 2\delta \end{pmatrix}$$
$$= \begin{pmatrix} E_{0+}^2 + E_{0-}^2 \\ 2E_{0+}E_{0-}\cos(\varphi_+ - \varphi_-) \\ 2E_{0+}E_{0-}\sin(\varphi_+ - \varphi_-) \\ E_{0+}^2 - E_{0-}^2 \end{pmatrix}. \quad (8)$$

Combined with Eqs. (5)–(8), the Faraday rotation and the ellipticity of the exiting probe light are

$$\theta = \frac{1}{2}(\varphi_+ - \varphi_-)$$
$$= \frac{\omega_{\text{probe}}L}{4c}\text{Re}(\chi_+ - \chi_-), \quad (9)$$

$$\sin 2\delta = \frac{E_{0+}^2 - E_{0-}^2}{E_{0+}^2 + E_{0-}^2}$$
$$= \frac{1 - \exp\left(\frac{\omega_{\text{probe}}L}{c}\text{Im}(\chi_+ - \chi_-)\right)}{1 + \exp\left(\frac{\omega_{\text{probe}}L}{c}\text{Im}(\chi_+ - \chi_-)\right)}. \quad (10)$$

It is worth noting that our theory model is based on the linear two-photon absorption process. When the pumping effect is relatively strong, the nonlinear absorption of the pump light in the vapor cell needs to be considered and our theory is not applicable.

III. EXPERIMENTAL METHOD

Most of the studies used the balanced polarimetry to measure the Faraday rotation of the direct transitions of the atoms [13,15,33,34]. This method can only measure the rotation of the integer multiples of π and cannot avoid the errors caused by the ellipticity due to the circular dichroism [35,36]. Besides, the balanced polarimetry cannot measure the ellipticity.
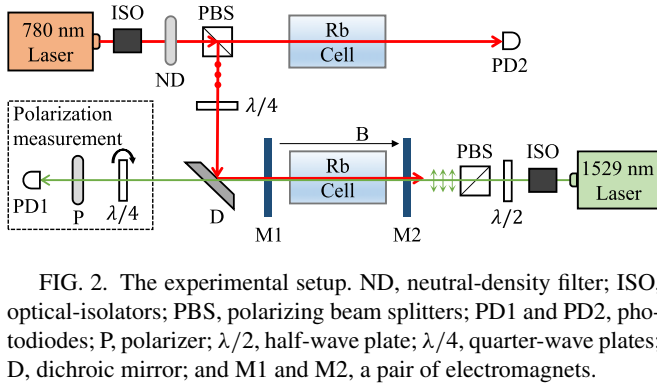
FIG. 2. The experimental setup. ND, neutral-density filter; ISO, optical-isolators; PBS, polarizing beam splitters; PD1 and PD2, photodiodes; P, polarizer; $\lambda/2$, half-wave plate; $\lambda/4$, quarter-wave plates; D, dichroic mirror; and M1 and M2, a pair of electromagnets.

Yingying Li *et al.* used a rotating polarizer to measure the ellipticity of the near-resonant probe light [36], which does not allow simultaneous measurement with probe light sweeping and cannot measure Faraday rotation at the same time. In this study, we used the rotating quarter-wave plate method [32] to measure the variation of the Stokes parameters with the frequency of the probe light in the vicinity of the rubidium $5P_{3/2} \rightarrow 4D_{5/2}$ transition, which can obtain the near-resonant Faraday rotation and the ellipticity spectra to analyze the polarization state. It is one of the most accurate methods available for simultaneously measuring the polarization rotation and ellipticity.

The rotating quarter-wave plate method [32] consists of a rotating quarter-wave plate, a polarizer, and a photodetector in Fig. 2. In the experiment, the rotation speed of the quarter wave plate was 75 cycles per second and the sampling and calculation were performed once per cycle, so the sampling rate was 75 Hz. The Faraday rotation and the ellipticity are calculated by Eqs. (11) and (12) upon the measured Stokes parameters:

$$\theta = \frac{1}{2}\tan^{-1}\left(\frac{S_2}{S_1}\right), \tag{11}$$

$$\sin 2\delta = \frac{S_3}{S_0}. \tag{12}$$

The experimental setup is shown in Fig. 2. The power of the pump light was varied using a neutral-density filter. A polarizing beam splitter divided the pump light into two linearly polarized beams, one entering the reference Rb vapor cell at room temperature and the other into another cell for pumping. A quarter-wave plate was added to the pump light path to change the pump light to circularly polarized light when needed. The power of the linearly polarized probe light was adjusted to 50 μW by a half-wave plate and a polarizing beam splitter. The pump light and the probe light of the counterpropagation configuration were converged in the cell by the dichroic mirror. The beam diameters of the pump light and the probe light were about 2.5 and 1 mm, respectively, to ensure that the pump light wraps around the probe light in the cell. In the experiment, when the pump light was linearly polarized, the polarization direction of the probe light and the pump light were perpendicular. The frequency of the pump light was aligned to the $5S_{1/2}(F_g = 3) \rightarrow 5P_{3/2}(F_e = 4)$ transition and the frequency of the probe light was swept in the vicinity of the $5P_{3/2} \rightarrow 4D_{5/2}$ transition.

The two vapor cells were filled with the natural rubidium atoms (72.17% ^{85}Rb and 27.83% ^{87}Rb). The temperature of
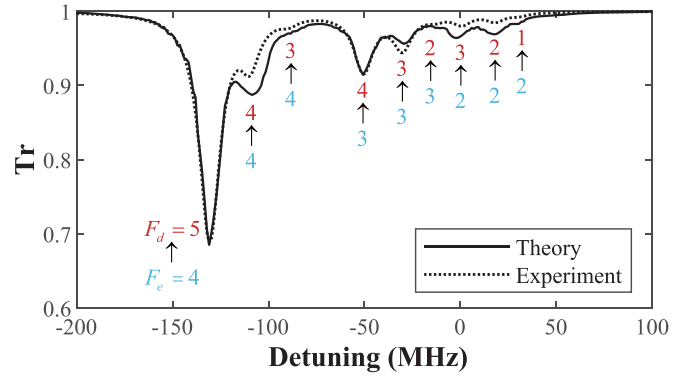

FIG. 3. The experimental and theoretical optical-optical double resonance (OODR) absorption spectra with no magnetic field. The temperature is 60 °C and the pump power is 0.5 mW. Here and in the following figures, Tr indicates the transmission of the probe light. The detuning of the probe light is with respect to the weighted $5P_{3/2} \rightarrow 4D_{5/2}$ transition line center (1529.37 nm).

the cell was stabilized by a feedback heating device. The relationship between the concentration of the rubidium atoms and the temperature is given in Ref. [29]. The cell length is $L = 3$ cm and the cell radius is $r = 1$ cm. A pair of the electromagnets M1 and M2 was used to produce the longitudinal magnetic field along the cell. The electromagnet has a radius of 10 cm to provide a uniform magnetic field. The magnetic field was controlled by the current through the electromagnets and measured by a Gauss meter with an inhomogeneity of less than 1% along the light path in the cell.

IV. THEORETICAL AND EXPERIMENTAL RESULTS

The experimental and theoretical OODR absorption spectra with no magnetic field are shown in Fig. 3. The selection rule for both $5S_{1/2} \rightarrow 5P_{3/2}$ and $5P_{3/2} \rightarrow 4D_{5/2}$ transitions is $\Delta F = 0, \pm 1$. The atoms are distributed in three hyperfine levels $F_e = 4, 3, 2$ of the $5P_{3/2}$ state due to the Doppler broadening of pumping. Under the selection rule, there are nine absorption peaks with the corresponding transitions already marked in the figure, where $5P_{3/2}(F_e = 4) \rightarrow 4D_{5/2}(F_d = 5)$ is a cycling transition that causes a strong absorption. Considering the wavelength mismatch effect, the counterpropagating configuration reduces the hyperfine splits of the $5P_{3/2}$ state to $(1 - \omega_{\text{probe}}/\omega_{\text{pump}})$ times of its original value. The two splits of the $5P_{3/2}(F_e = 4, 3, 2)$ hyperfine structures reduce from 120.7 and 63.4 MHz to 59.1 and 39.0 MHz, while the four splits of the hyperfine structures $4D_{5/2}(F_d = 5, 4, 3, 2, 1)$ remain unchanged at 20.8, 20.7, 17.8, and 13.0 MHz, respectively. The theoretical results are consistent with the experiment.

The longitudinal magnetic field breaks the degeneracy of levels and produces different frequencies due to the variation of the m_F angular momentum. The magnitude of the Zeeman splitting is proportional to the magnetic field. The selection rules for both $5S_{1/2} \rightarrow 5P_{3/2}$ and $5P_{3/2} \rightarrow 4D_{5/2}$ transitions are $\Delta F = 0, \pm 1$ and $\Delta m_F = \pm 1$. For the linearly polarized probe light, it can be considered as the superposition of the σ^- and σ^+ circularly polarized components, where the σ^- component corresponds to the $\Delta m_F = -1$ transitions of the upper
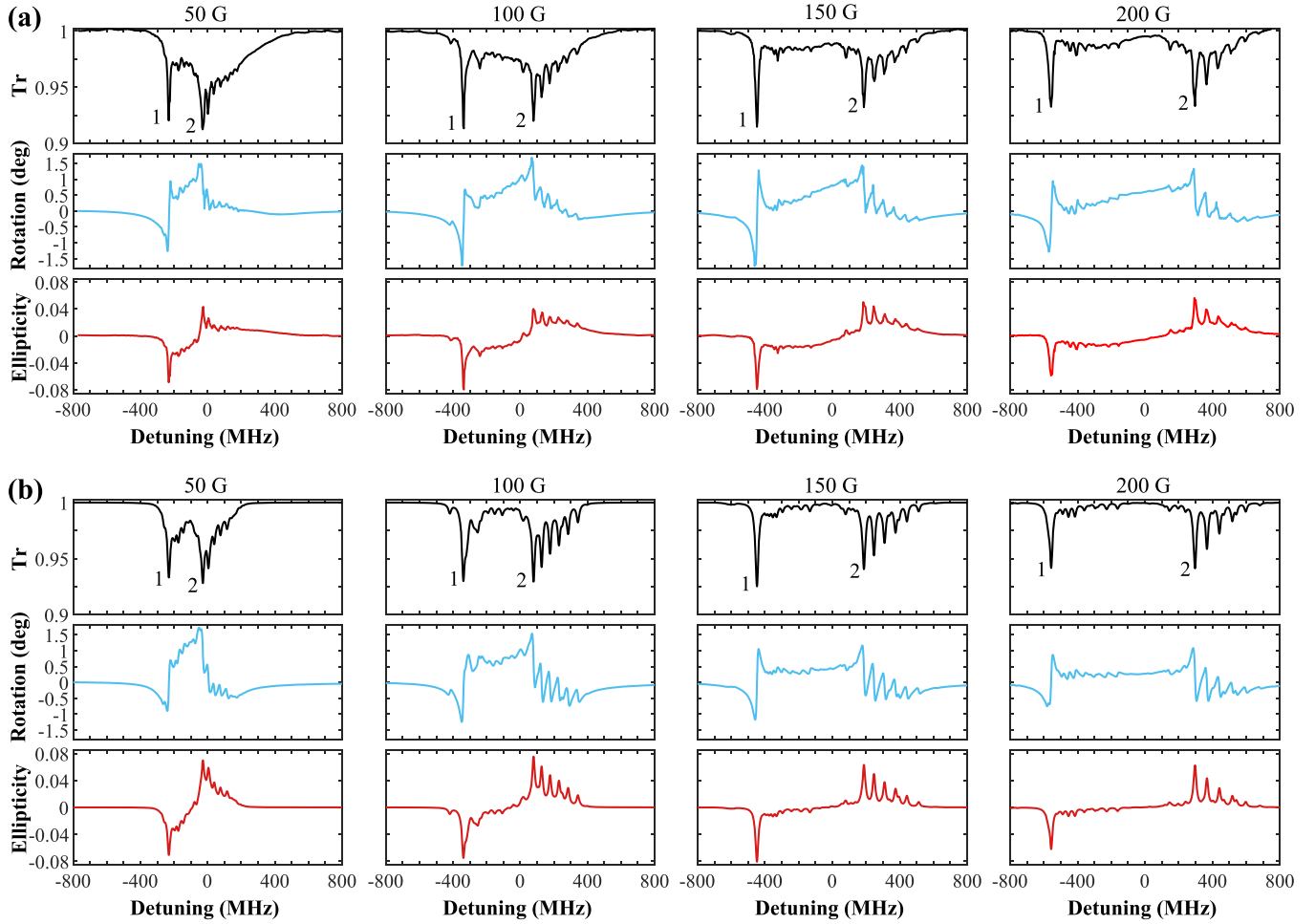
FIG. 4. The (a) experimental and (b) theoretical absorption, rotation, and ellipticity spectra of rubidium $5P_{3/2} \rightarrow 4D_{5/2}$ transition in different magnetic fields. The temperature is 80 °C and the pump power is 0.5 mW. The first row, second row, and third row represent the absorption, rotation, and ellipticity spectra, respectively. The different magnetic fields represented by each column have been indicated in the figure.

and the lower levels, and the σ^+ component corresponds to the $\Delta m_F = +1$ transitions. The absorption and dispersion of the σ^- and σ^+ circularly polarized components are different for the same frequency of the probe light due to the splitting of the m_F sublevels caused by the Zeeman effect. The different absorption results in different amplitudes of the σ^- and σ^+ circularly polarized components, while the different dispersion results in different phases. The probe light exiting the cell can be regarded as the superposition of the σ^- and σ^+ circularly polarized components which have different amplitudes, different phases and the same frequency. The different phases lead to the polarization rotation, while the different amplitudes lead to the ellipticity.

The experimental and theoretical absorption, rotation, and ellipticity spectra in different magnetic fields are shown in Fig. 4. Even though these spectra are complicated due to the numerous Zeeman sublevels, regularities can still be seen in some sublevels with high transition probabilities. Under the magnetic field of 50 G, the first high absorption peak appears at the detuning of about -220 MHz, labeled 1 in figures. The branching sublevel of this absorption peak is

$F_g = 3(m_{F_g} = 3) \rightarrow F_e = 4(m_{F_e} = 2) \rightarrow F_d = 4(m_{F_d} = 3)$, where $\Delta m_F = +1$ corresponds to the absorption of the σ^+ circularly polarized component. Consequently, the negative ellipticity appears at this frequency point with the same trend as the absorption spectra. The dispersion of the σ^+ circularly polarized component varies while the dispersion of the σ^- component is basically unchanged, which corresponds to the negative and then positive change of the polarization rotation in the figure. Subsequently, the second high absorption peak appears at the detuning of about -30 MHz, labeled 2. The branching sublevel is $F_g = 3(m_{F_g} = -1) \rightarrow F_e = 3(m_{F_e} = 0) \rightarrow F_d = 4(m_{F_d} = -1)$, where $\Delta m_F = -1$ corresponds to the absorption of the σ^- component. The several high absorption peaks following this peak are also the $\Delta m_F = -1$ transitions. Therefore, the polarization rotation and ellipticity behave in the opposite way to that of the first absorption peak, with the positive ellipticity and the positive and then negative change of the polarization rotation.

As the magnetic field increases, it can be seen from the Fig. 4 that the frequency positions of the first absorption peak
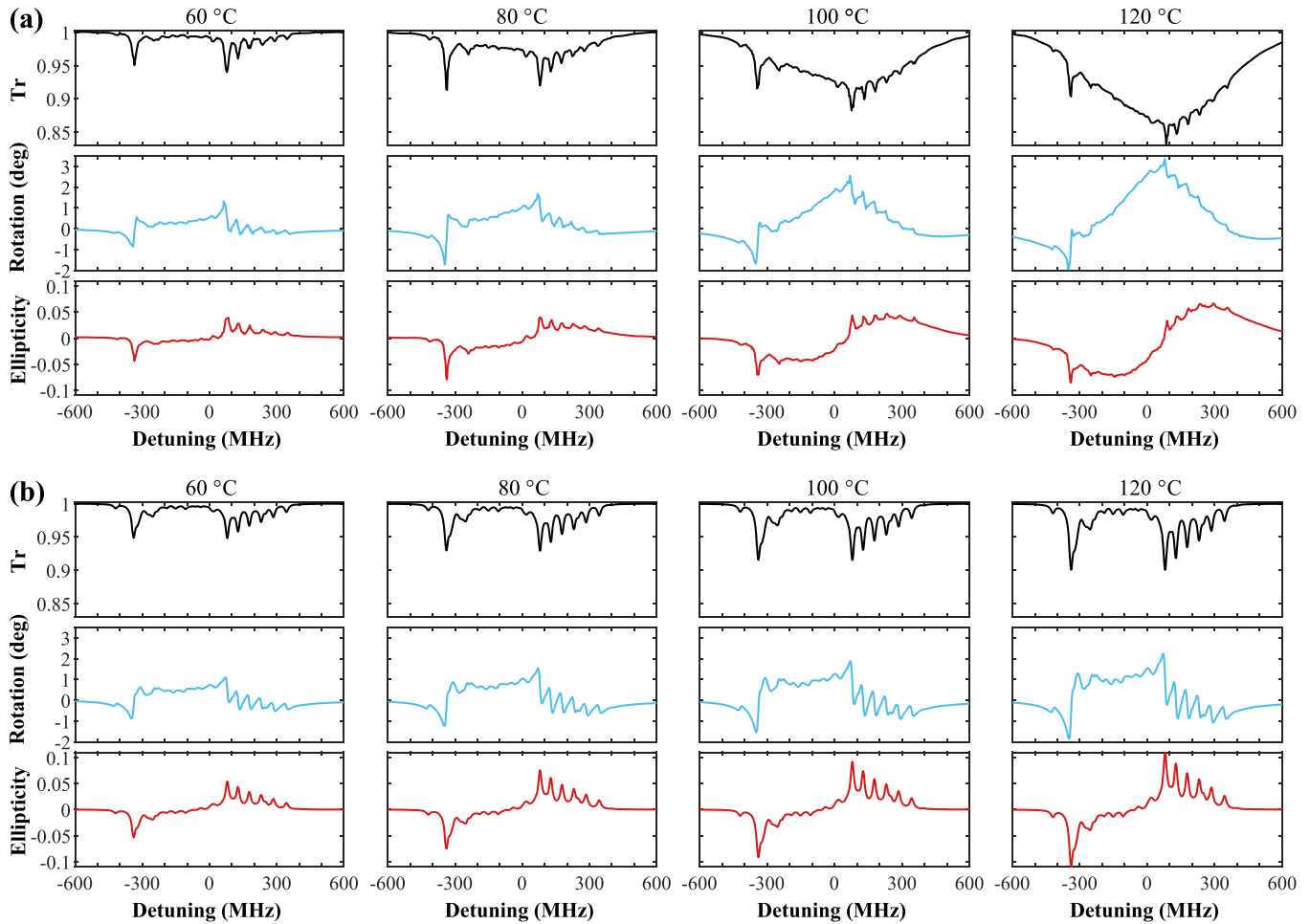
FIG. 5. The (a) experimental and (b) theoretical absorption, rotation, and ellipticity spectra of rubidium $5P_{3/2} \rightarrow 4D_{5/2}$ transition in different temperatures. The magnetic field is 100 G and the pump power is 0.5 mW. The different temperatures represented by each column have been indicated in the figure.

are about -220, -335, -450, and -565 MHz and of the second absorption peak are about -30, 80, 190, and 300 MHz, corresponding to 50, 100, 150, and 200 G magnetic fields. The magnitude of the Zeeman splittings varies essentially linearly with the magnetic field. Our theory can recover the experimental curves. Owing to the Doppler width of pumping, the pumping efficiency for individual sublevels decreases when the Zeeman splitting becomes larger, so there is a slight reduction in the absorption of probe light with the magnetic field increasing.

In the measurement of high-precision spectra such as optical-optical double resonance (OODR) and double resonance optical pumping (DROP) [37–41], the relatively low pump power (<5 mW) and low temperature (50–70 °C) were used for most of the studies in order to reduce the pump nonlinear effects as well as improve the SNR of the spectra. However, the concentration of the intermediate excited state atoms is too low to achieve a large polarization rotation in those cases. Therefore, the study of the case of higher temperature and higher pump optical power is important for the polarization state control of the optical signal between excited states of atoms.

The experimental and theoretical curves in different temperatures are shown in Fig. 5. The rise in temperature elevates

the concentration of rubidium atoms and increases the pump effect, which enhances the susceptibility and leads to the simultaneous increase of the circular birefringence and the circular dichroism in the vapor cell.

The raised temperature increases the nonlinear effects in the cell, such as the energy pooling process [42], which has an impact on pumping process. The theoretical model in this paper only considers the linear two-photon absorption process, so the deviation between experimental and theoretical results becomes large at a high temperature. As the temperature raises, the atoms of intermediate excited state atom appear to have the same Maxwell velocity distribution as the ground state, leading to the Doppler broadening of the absorption of the probe light. At a temperature of 120 °C in Fig. 5, each Zeeman sublevel exhibits a Lorentzian broadening superimposed on the overall Doppler broadening. The effects of Doppler broadening and Lorentz broadening of the Zeeman sublevels on the absorption, rotation, and ellipticity spectra can be clearly distinguished. The spectra is similar to that of electromagnetically induced absorption, but its principle is different.

Comparing the experimental curves at different temperatures, it can also be seen that the rise in temperature leads to little variation in the Lorentzian broadening of the Zeeman
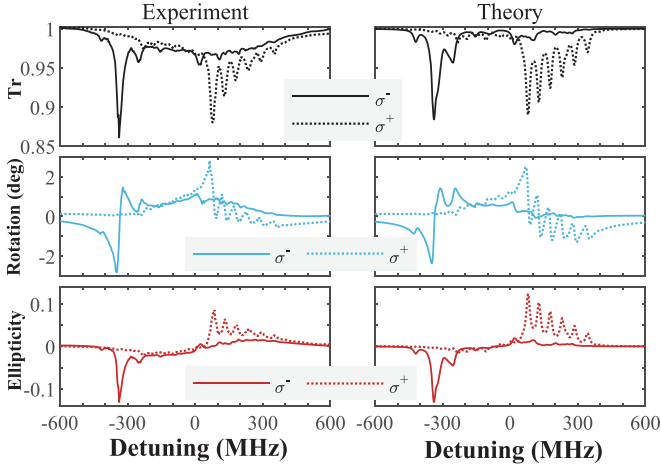
FIG. 6. The absorption, rotation, and ellipticity spectra of rubidium $5P_{3/2} \rightarrow 4D_{5/2}$ transition of the σ^- and σ^+ circularly polarized pump light. The temperature is 80 °C, the magnetic field 100 Gs, and the pump power 0.5 mW. The first and second columns present the experimental and theoretical curves, respectively.

sublevels. The reason is the Lorentzian linewidth between excited states of atoms is only affected by the natural linewidths of the transitions and the linewidths of the pump laser and the probe laser [37].

In Fig. 6, we used a quarter-wave plate to change the pump light into the σ^- and σ^+ circularly polarized light of the same pump power, observing the pump light for the $\Delta m_F = -1, +1$ Zeeman sublevels separately. Compared with the scenario of linearly polarized pump light, the sublevels pumped to the intermediate excited states are half less. The simpler optical choice makes the spectra cleaner. The superimposed spectra of the σ^- and σ^+ circularly polarized pump light in Fig. 6 is the same as in Fig. 4 under the magnetic field of 100 G.

V. POLARIZATION ROTATION CONTROL

The experimental curves in different pump powers are shown in Fig. 7. The raise in pump power increases the pump effect significantly, leading to a simultaneous increase in Faraday rotation and ellipticity, which also leads to a gradual overshadowing of the Zeeman sublevels. At the pump power of 50 mW (dark red line with inverted triangle), the absolute value of the ellipticity is close to 1 at the maximum, indicating that the exiting probe light at that frequency point becomes almost circularly polarized light.

The Autler-Townes effect in the OODR absorption spectra of the raising pump power has been reported experimentally and theoretically [38,43]. In our work, the Autler-Townes splitting can also be clearly observed in some specific Zeeman sublevels with strong absorption, which has been marked in the figure. Futhermore, the Autler-Townes effect can also be observed in the Faraday rotation and the ellipticity spectra.

The frequency width of the $5P_{3/2} \rightarrow 4D_{5/2}$ hyperfine splitting without magnetic field is 188 MHz in Fig. 3, which corresponds to the Zeeman splitting at a magnetic field of about 120 G. The Zeeman effect dominates when the magnetic
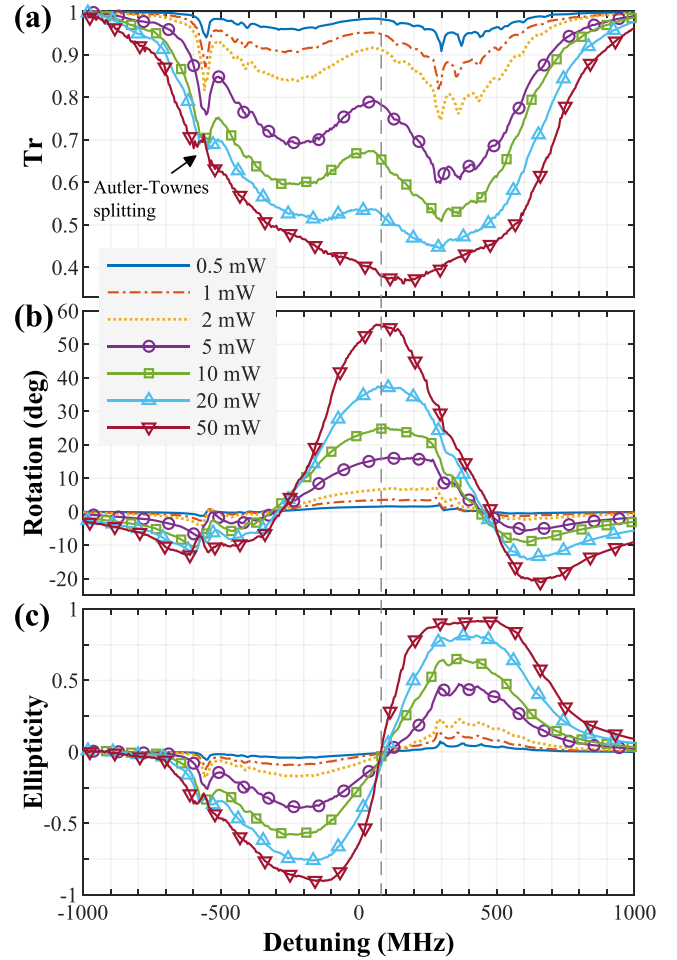

FIG. 7. Experimental (a) absorption, (b) rotation, and (c) ellipticity spectra of rubidium $5P_{3/2} \rightarrow 4D_{5/2}$ transition in different pump power. The magnetic field is 200 G and the temperature is 100 °C.

field is 200 G in Fig. 7. The absorption of σ^- and σ^+ circularly polarized component is partially separated in the relatively strong magnetic fields. The absorption of the σ^- circularly polarized component is dominant on the left side of the vertical gray dashed line, while the absorption of the σ^+ component is dominant on the right side. At the frequency point of the gray dashed line, the absorptions of the σ^- and σ^+ components are equal so the ellipticity is zero and also corresponds to the recess in the absorption spectra.

At the frequency point corresponding to the vertical gray dashed line, the rotation angle is over 50 deg, and the ellipticity is zero of the pump power 50 mW. Therefore, we obtained the polarization rotation for more than 50 deg with negligible elliptical distortion of the 1529 nm near-resonant light. More rotation angle can be obtained by raising pump power and temperature, but it will cause more absorption, so the balance between the polarization rotation and absorption must be taken into consideration.

It can be observed that the rise in pump power has little effect on the frequency point where the ellipticity is zero, so it is available to achieve the polarization rotation control of the 1529-nm near-resonant light by the variation of the pump power at the frequency points of the vertical gray dashed line

in the figure. Although a 50-deg polarization rotation is not well suitable for the application of the all optical switching, it is sufficient for the application of the dynamic half-wave plate [44]. In addition, the ellipticity varies monotonically with the pump power at the maximum points to the left and right side of the vertical gray dashed line, which can be applied to the dynamic quarter-wave plate.

However, there are two problems with this polarization rotation method. First, unlike the off-resonant polarization rotation method, the absorption of the probe light at this frequency point is strong. The maximum absorption of the probe light is up to more than 60% under the pump power of 50 mW in the experiment. Second, this method requires high-frequency stability of the probe light. The instability of the probe light frequency may cause a surge of the elliptical distortion in polarization rotation. We believe that the performance of this method can be made better in further studies, for example, by choosing the appropriate magnetic field for different temperatures and pump powers.

VI. CONCLUSION

In conclusion, we have calculated and experimentally measured the Faraday rotation and ellipticity spectra of rubidium $5P_{3/2} \rightarrow 4D_{5/2}$ transition in a magnetic field. Considering the wavelength mismatch effect and the Doppler effect of pumping, the theoretical calculation is demonstrated. In the experiment, the rotating quarter-wave plate method is used to measure the Faraday rotation and the ellipticity spectra of the near-resonant probe light simultaneously. The theory can recover the experimental curves when the nonlinear effect of pumping is weak. We obtained the polarization rotation between excited states of rubidium atoms over 50 deg with negligible elliptical distortion experimentally. By analyzing the rotation and the ellipticity spectra, we propose the potential of the polarization rotation control of the 1529-nm near-resonant light by varied pump power. The polarization rotation of 1529-nm wavelength can be used for all-optical networks and quantum communications in the 1.5-μm waveband. We believe our study have provided enlightenments for an understanding of the polarization rotation of the Faraday effect between excited states of atoms and provides more adaptable scenarios for optical devices using Faraday effect.

ACKNOWLEDGMENTS

APPENDIX: DETAILS OF THE TRANSITION PROBABILITY CALCULATION

Using the coupled basis $|I, J, F, m_F\rangle$, the total Hamiltonian of the atomic system in an in an external magnetic field can be written as [40]

$$H = H_0 + H_{\text{fs}} + H_{\text{hfs}} + H_B, \tag{A1}$$

where H_0 is the coarse atomic structure, H_{fs} and H_{hfs} characterizes the fine and the hyperfine structure, and H_B represents the atomic interaction with the external magnetic field. The hyperfine structure and the atomic interaction with the external magnetic field can be seen as the perturbed Hamiltonian on the basis of fine structures of the atomic system.

Considering the magnetic dipole moment and the electric quadrupole moment, the hyperfine structure can be described as

$$H_{\text{hfs}} = \frac{A_{\text{hfs}}}{2}K + \frac{B_{\text{hfs}}}{4}\frac{\frac{3}{2}K(K+1) - 2I(I+1)J(J+1)}{I(2I-1)(2J-1)}, \tag{A2}$$

where A_{hfs} and B_{hfs} are the hyperfine structure constants and its data are taken from Refs. [28,41,45], $K = F(F+1) - I(I+1) - J(J+1)$. H_B characterizes Zeeman effect under the longitudinal magnetic field B_z,

$$H_B = \frac{\mu_B}{\hbar}(g_J \mathbf{J} + g_I \mathbf{I}) \cdot \mathbf{B}, \tag{A3}$$

where μ_B is the Bohr magneton, $\hbar$ is the reduced Planck constant, and g_J and g_I are Landé g factors depend on J and I, respectively. The two terms are expressed as

$$\langle IJF_i m_{F_i}|g_J \mathbf{J} \cdot \mathbf{B}|IJF_j m_{F_j}\rangle$$
$$= g_J B_z (-1)^{I+J+F_i+F_j-m_F+1}$$
$$\times \sqrt{(2F_i+1)(2F_j+1)J(J+1)(2J+1)}$$
$$\times \begin{pmatrix} F_i' & 1 & F_j \\ -m_F & 0 & m_F \end{pmatrix}\begin{Bmatrix} J & F_i & I \\ F_j & J & 1 \end{Bmatrix}, \tag{A4}$$

$$\langle IJF_i m_{F_i}|g_I \mathbf{I} \cdot \mathbf{B}|IJF_j m_{F_j}\rangle$$
$$= g_I B_z (-1)^{I+J+F_i+F_j-m_F+1}$$
$$\times \sqrt{(2F_i+1)(2F_j+1)I(I+1)(2I+1)}$$
$$\times \begin{pmatrix} F_i' & 1 & F_j \\ -m_F & 0 & m_F \end{pmatrix}\begin{Bmatrix} I & F_i & J \\ F_j & I & 1 \end{Bmatrix}, \tag{A5}$$

where i and j are different sublevels of Zeeman effect. The quantities in brackets are $3j$ symbols and in curled bracket $6j$ symbols.

The full matrix $\langle I, J, F, m_F|H|I, J, F, m_F\rangle$ of the ground state, the intermediate excited state, and the doubly excited state are diagonalized separately to obtain the eigenvalues and eigenstates of those three states. The eigenvalues describe the transition frequencies between the upper and lower sublevels, and the eigenvectors V_g, V_e, and V_d are represented by a mapping of the basis $|I, J, F, m_F\rangle$,

$$V_g = \sum_{F_g, m_{F_g}} C_g |I_g, J_g, F_g, m_{F_g}\rangle. \tag{A6}$$

This equation also applies to the e and d states.

The transition probability of the basis $|F, m_F\rangle$ between the upper and lower levels is

$$\sigma_{m_F m_{F'}} = \langle F, m_F|e\mathbf{r}|F', m_{F'}\rangle$$
$$= \begin{pmatrix} F' & 1 & F \\ m_{F'} & m_{F'}-m_F & -m_F \end{pmatrix}\begin{Bmatrix} J & J' & 1 \\ F' & F & I \end{Bmatrix}$$
$$\times \langle J|e\mathbf{r}|J'\rangle(-1)^{2F'+I+J+m_F}$$
$$\times \sqrt{(2F+1)(2F'+1)(2J+1)}, \tag{A7}$$

where $F \rightarrow F'$ represents the $F_g \rightarrow F_e$ or the $F_e \rightarrow F_d$ transition. Here $m_{F'} - m_F = 1, -1$ represent the σ^+ and σ^- circularly polarized light, respectively. The value of the reduced matrix element $\langle J|e\mathbf{r}|J'\rangle$ is the same for the same $F \rightarrow F'$ transition and can be calculated using the expression for the decay rate Γ [29]:

$$\Gamma = \frac{16\pi^3}{3\epsilon_0 h \lambda_0{}^3} \frac{2J+1}{2J'+1} \langle J|e\mathbf{r}|J'\rangle^2, \quad (A8)$$

where ϵ_0 is the vacuum permittivity and λ_0 is the is the wavelength of the corresponding transition.

The transition probability of the eigenvectors of the $g \rightarrow e$ states can be described as

$$\sigma_{ge} = \sum_{F_g, m_{F_g}} \sum_{F_e, m_{F_e}} C_g C_e \sigma_{m_{F_g} m_{F_e}}. \quad (A9)$$

This equation also applies to the eigenvectors of the $e \rightarrow d$ states.

[1] S. Manipatruni, J. T. Robinson, and M. Lipson, Optical Nonreciprocity in Optomechanical Structures, Phys. Rev. Lett. **102**, 213903 (2009).

[2] C. Liang, B. Liu, A.-N. Xu, X. Wen, C. Lu, K. Xia, M. K. Tey, Y.-C. Liu, and L. You, Collision-Induced Broadband Optical Nonreciprocity, Phys. Rev. Lett. **125**, 123901 (2020).

[3] L. Del Bino, J. M. Silver, M. T. Woodley, S. L. Stebbings, X. Zhao, and P. Del'Haye, Microresonator isolators and circulators based on the intrinsic nonreciprocity of the Kerr effect, Optica **5**, 279 (2018).

[4] X.-W. Xu and Y. Li, Optical nonreciprocity and optomechanical circulator in three-mode optomechanical systems, Phys. Rev. A **91**, 053854 (2015).

[5] D. Jalas, A. Petrov, M. Eich, W. Freude, S. Fan, Z. Yu, R. Baets, M. Popović, A. Melloni, J. D. Joannopoulos *et al.*, What is—and what is not—an optical isolator, Nat. Photon. **7**, 579 (2013).

[6] Y. Tian, Y. Fu, and J. Zhang, Transformer-based under-sampled single-pixel imaging, Chin. J. Electron. **32**, 1 (2023).

[7] Y. Tian, Y. Fu, and J. Zhang, Joint supervised and unsupervised deep learning method for single-pixel imaging, Opt. Laser Technol. **162**, 109278 (2023).

[8] H. J. Kimble, The quantum internet, Nature (London) **453**, 1023 (2008).

[9] P. Lodahl, S. Mahmoodian, S. Stobbe, A. Rauschenbeutel, P. Schneeweiss, J. Volz, H. Pichler, and P. Zoller, Chiral quantum optics, Nature (London) **541**, 473 (2017).

[10] C. Caloz, A. Alu, S. Tretyakov, D. Sounas, K. Achouri, and Z.-L. Deck-Léger, Electromagnetic Nonreciprocity, Phys. Rev. Appl. **10**, 047001 (2018).

[11] L. Bi, J. Hu, P. Jiang, D. H. Kim, G. F. Dionne, L. C. Kimerling, and C. Ross, On-chip optical isolation in monolithically integrated non-reciprocal optical resonators, Nat. Photon. **5**, 758 (2011).

[12] P. Pershan, Magneto-optical effects, J. Appl. Phys. **38**, 1482 (1967).

[13] P. Siddons, N. C. Bell, Y. Cai, C. S. Adams, and I. G. Hughes, A gigahertz-bandwidth atomic probe based on the slow-light Faraday effect, Nat. Photon. **3**, 225 (2009).

[14] Z. Chai, X. Hu, F. Wang, X. Niu, J. Xie, and Q. Gong, Ultrafast all-optical switching, Adv. Opt. Mater. **5**, 1600665 (2017).

[15] P. Siddons, C. S. Adams, and I. G. Hughes, Optical control of Faraday rotation in hot Rb vapor, Phys. Rev. A **81**, 043838 (2010).

[16] T. Dannegger, M. Berritta, K. Carva, S. Selzer, U. Ritzmann, P. M. Oppeneer, and U. Nowak, Ultrafast coherent all-optical switching of an antiferromagnet with the inverse Faraday effect, Phys. Rev. B **104**, L060413 (2021).

[17] M. O. A. Ellis, E. E. Fullerton, and R. W. Chantrell, All-optical switching in granular ferromagnets caused by magnetic circular dichroism, Sci. Rep. **6**, 30522 (2016).

[18] N. Korneev and J. Soto, The nonlinear Faraday rotation-based dynamic holography in rubidium vapor, Opt. Commun. **245**, 437 (2005).

[19] R. P. Abel, U. Krohn, P. Siddons, I. G. Hughes, and C. S. Adams, Faraday dichroic beam splitter for Raman light using an isotopically pure alkali-metal-vapor cell, Opt. Lett. **34**, 3071 (2009).

[20] G. P. Agrawal, *Fiber-Optic Communication Systems* (John Wiley & Sons, New York, 2012).

[21] A. Mokhtar and M. Azizoglu, Adaptive wavelength routing in all-optical networks, IEEE/ACM Trans. Networking **6**, 197 (1998).

[22] S. Wielandy and A. L. Gaeta, Coherent Control of the Polarization of an Optical Field, Phys. Rev. Lett. **81**, 3359 (1998).

[23] R. Drampyan, S. Pustelny, and W. Gawlik, Electromagnetically induced transparency versus nonlinear Faraday effect: Coherent control of light-beam polarization, Phys. Rev. A **80**, 033815 (2009).

[24] L.-W. Luo, N. Ophir, C. P. Chen, L. H. Gabrielli, C. B. Poitras, K. Bergmen, and M. Lipson, WDM-compatible mode-division multiplexing on a silicon chip, Nat. Commun. **5**, 3069 (2014).

[25] S. Liao, H.-L. Yong, C. Y. Liu, G. Shentu, D.-D. Li, J. Lin, H. Dai, S.-Q. Zhao, B. Li, J.-Y. Guan, W. Chen, Y.-H. Gong, Y. Li, Z. Lin, G.-S. Pan, J. S. Pelc, M. M. Fejer, W. Z. Zhang, W. Liu, J. Yin, J.-G. Ren, X. Wang, Q. Zhang, C.-Z. Peng, and J.-W. Pan, Long-distance free-space quantum key distribution in daylight towards inter-satellite communication, Nat. Photon. **11**, 509 (2017).

[26] N. Gisin and R. Thew, Quantum communication, Nat. Photon. **1**, 165 (2007).

[27] M. Atatüre, J. Dreiser, A. Badolato, and A. Imamoglu, Observation of Faraday rotation from a single confined spin, Nat. Phys. **3**, 101 (2007).

[28] C. Liu, Y. Hai, and A. Dang, Optically end-pumped scheme in rubidium vapor: Theory and experiment, Appl. Phys. Lett. **121**, 101102 (2022).

[29] P. Siddons, C. S. Adams, C. Ge, and I. G. Hughes, Absolute absorption on rubidium D lines: Comparison between theory and experiment, J. Phys. B: At. Mol. Phys. **41**, 155004 (2008).

[30] E. Talker, L. Stern, A. Naiman, Y. Barash, and U. Levy, Fluorescence double resonance optical pumping spectrum and its application for frequency stabilization in millimeter scale vapor cells, J. Phys. Commun. **1**, 055016 (2017).

[31] D. Meschede, *Optics, Light and Lasers: The Practical Approach to Modern Aspects of Photonics and Laser Physics* (John Wiley & Sons, 2017).

[32] B. Schaefer, E. Collett, R. Smyth, D. Barrett, and B. Fraher, Measuring the Stokes polarization parameters, Am. J. Phys. **75**, 163 (2007).

[33] A. L. Marchant, S. Händel, T. P. Wiles, S. A. Hopkins, C. S. Adams, and S. L. Cornish, Off-resonance laser frequency stabilization using the Faraday effect, Opt. Lett. **36**, 64 (2011).

[34] D. A. Van Baak, Resonant Faraday rotation as a probe of atomic dispersion, Am. J. Phys. **64**, 724 (1996).

[35] W. Demtröder, *Laser spectroscopy 2: Experimental techniques* (Springer, 2015).

[36] Y. Li, Z. Wang, S. Jin, J. Yuan, and H. Luo, Elliptical polarization of near-resonant linearly polarized probe light in optically pumped alkali metal vapor, Sci. Rep. **7**, 43066 (2017).

[37] M. Breton, N. Cyr, P. Tremblay, M. Tetu, and R. Boucher, Frequency locking of a 1324 nm DFB laser to an optically pumped rubidium vapor, IEEE Trans. Instrum. Meas. **42**, 162 (1993).

[38] A. Nishiyama, S. Yoshida, Y. Nakajima, H. Sasada, K. Nakagawa, A. Onae, and K. Minoshima, Doppler-free dual-comb spectroscopy of Rb using optical-optical double resonance technique, Opt. Express **24**, 25894 (2016).

[39] C.-L. Hu, V. I. Perevalov, C.-F. Cheng, T.-P. Hua, A.-W. Liu, Y. R. Sun, Y. Tan, J. Wang, and S.-M. Hu, Optical-optical double-resonance absorption spectroscopy of molecules with khz accuracy, J. Phys. Chem. Lett. **11**, 7843 (2020).

[40] Z. S. Xu, M. H. Cai, S. H. You, S. S. Zhang, and H. P. Liu, Optical-optical double resonance spectroscopy of Rb $5D_{3/2,5/2}$ in magnetic fields, Spectrochim. Acta **193**, 106453 (2022).

[41] J. Wang, H. Liu, G. Yang, B. Yang, and J. Wang, Determination of the hyperfine structure constants of the 87 Rb and 85 Rb 4 *d* 5 /2 state and the isotope hyperfine anomaly, Phys. Rev. A **90**, 052505 (2014).

[42] L. Barbier and M. Cheret, Energy pooling process in rubidium vapour, J. Phys. B **16**, 3213 (1983).

[43] H. R. Gray and C. R. Stroud, Autler-Townes effect in double optical resonance, Opt. Commun. **25**, 359 (1978).

[44] S. Li, B. Wang, X. Yang, Y. Han, H. Wang, M. Xiao, and K.C. Peng, Controlled polarization rotation of an optical field in multi-Zeeman-sublevel atoms, Phys. Rev. A **74**, 033821 (2006).

[45] D. A. Steck, Rubidium 85 *d* line data, http://steck.us/alkalidata.